Multiple pathways for the formation of secondary organic aerosol in North China Plain in summer

Yifang Gu[1,4], Ru-Jin Huang[1,2,3,4], Jing Duan[1], Wei Xu[1], Chunshui Lin[1], Haobin Zhong[1,4], Ying Wang[1], Haiyan Ni[1], Quan Liu[5], Ruiguang Xu[6,7], Litao Wang[6,7], Yong Jie Li[8]

[1]SKLLQG, Center for Excellence in Quaternary Science and Global Change, Institute of Earth Environment, Chinese Academy of Sciences, Xi'an 710061, China

[2]Open Studio for Oceanic-Continental Climate and Environment Changes, Pilot National Laboratory for Marine Science and Technology (Qingdao), Qingdao 266000, China

[3]Institute of Global Environmental Change, Xi'an Jiaotong University, Xi'an 710049, China

[4]University of Chinese Academy of Sciences, Beijing 100049, China

[5]State Key Laboratory of Severe Weather & Key Laboratory of Atmospheric Chemistry of C MA, Chinese Academy of Meteorological Sciences, Beijing 100081, China

[6]Department of Environmental Engineering, School of Energy and Environmental Engineering, Hebei University of Engineering, Handan 056038, China

[7]Hebei Key Laboratory of Air Pollution Cause and Impact, Handan 056038, China

[8]Department of Civil and Environmental Engineering, and Centre for Regional Oceans, Faculty of Science and Technology, University of Macau, Taipa, Macau 999078, China

Correspondence to: Ru-Jin Huang (rujin.huang@ieecas.cn)

Abstract

Secondary organic aerosol (SOA) has been identified as a major contributor to fine particulate matter ($PM_{2.5}$) in North China Plain (NCP). However, the chemical mechanisms involved are still unclear due to incomplete understanding of its multiple formation processes. Here we report field observations in summer in Handan of NCP, based on high-resolution online measurements. Our results reveal the formation of SOA via photochemistry and two types of aqueous-phase chemistry, the latter of which include nocturnal and daytime processing. The photochemical pathway is the most important under high O_x ($=O_3 + NO_2$) conditions (65.1 ± 20.4 ppb). The efficient SOA formation from photochemistry (O_x-initiated-SOA) dominated the daytime (65% to OA) with an average growth rate of 0.8 $\mu g\ m^{-3}\ h^{-1}$. During the high relative humidity (RH: 83.7 ± 12.5 %) period, strong nocturnal aqueous-phase SOA formation (aq-SOA) played a significant role in SOA production (45% to OA) with a nighttime growth rate of 0.6 $\mu g\ m^{-3}\ h^{-1}$. Meanwhile, an equally fast growth rate of 0.6 $\mu g\ m^{-3}\ h^{-1}$ of O_x-initiated-SOA from daytime aqueous-phase photochemistry was also observed, which contributed 39% to OA, showing that photochemistry in the aqueous phase is also a non-negligible pathway in summer. The primary-related-SOA (SOA attributed to primary particulate organics) and aq-SOA are related to residential coal combustion activities, supported by distinct fragments from polycyclic aromatic hydrocarbons (PAHs). Moreover, the conversion and rapidly oxidation of primary-related-SOA to aq-SOA could be possible in the aqueous phase under high-RH conditions. This work sheds light on the multiple formation pathways of SOA in ambient air of complex pollution, and improves our understanding of ambient SOA formation and aging in summer with high oxidation capacity.

KEYWORDS: secondary organic aerosol, aqueous-phase chemistry, photochemistry, multiple-phase chemistry, complex air pollution

1. Introduction

Rapid economic growth and urbanization processes have led to severe particulate air pollution in China, affecting air quality, climates and human health (Huang et al., 2014; Cohen et al., 2017; An et al., 2019). Organic aerosol (OA) is a major component of aerosol particles, consisting of 20-90% of fine particle mass (Jimenez et al., 2009; Zhang et al., 2011). OA is either emitted directly from primary sources (referred to as primary OA, POA) such as traffic, cooking, coal combustion, and biomass burning, or produced through gas-to-particle conversion (referred to as secondary OA, SOA) in the atmosphere. In recent years, with the implementation of control measures, the POA fraction is decreasing and SOA fraction is increasing in North China Plain (NCP), indicating that SOA is becoming more critical for urban air quality (Huang et al., 2019; Xu et al., 2019; Gu et al., 2020). However, our understanding of the formation mechanisms and evolution processes of SOA is still limited.

Generally, SOA can be formed through gas-phase photochemical oxidation of volatile organic compounds (VOCs) followed by nucleation or condensation of oxidation products onto the preexisting particles (Donahue et al., 2006). Herndon et al., (2008) showed that oxygenated organic aerosol (OOA), a surrogate of SOA, was well correlated with odd oxygen ($O_x = O_3 +$ nitrogen dioxide (NO_2)) during photochemical processing. SOA can also be formed in the aqueous phase on wet aerosols, clouds and fogs through further chemical processes of water-soluble organic compounds or organic products of gas-phase photochemistry (Ervens et al., 2011, 2014). A growing number of laboratory studies and field measurements have indicated that aqueous-phase processes contribute efficiently to the formation of SOA (Gilardoni et al., 2016; Bikkina et al., 2017). However, how photochemistry and aqueous-phase chemistry coordinate to affect the formation of SOA is still unclear, despite numerous measurements to explore this question using aerosol chemical speciation monitor (ACSM) or aerosol mass spectrometer (AMS) (Hu et al., 2016b; Hu et al., 2017; Sun et al., 2016; Li et al., 2017; Sun et al., 2018b; Huang et al., 2019; Gu et al. 2020; Kuang et al., 2020). Field measurements in Beijing suggested that gas-phase photochemical oxidation can play a dominant role in SOA formation (Sun et al., 2016; Hu et al., 2016a). Xu et al., (2017) showed that less oxidized-OOA (LO-OOA) was mainly formed through photochemical oxidation, while the more oxidized-OOA (MO-OOA) formation was dominantly formed by aqueous-phase chemistry in Beijing for different seasons. Kuang et al. (2020) investigated the effects of gas-phase and aqueous-phase photochemical processes on the formation of SOA and found that photochemical aqueous-phase SOA formation dominantly contributed to daytime OOA formation in winter Gucheng, located between Beijing (~100 km) and Baoding (~40 km) on the NCP. We found that photochemical processing attributed mostly to MO-OOA in summertime Beijing (Gu et al., 2020). Although these studies provided important insights into SOA formation processes, our understanding on the photochemical and aqueous-phase formation pathways for SOA and their

impacts on oxidation degree are far from complete. This lack of understanding is especially so under the conditions that atmospheric oxidative capacity and pollution characteristics have been largely changing in China due to large reduction in direct emissions of air pollutants.

In this study, we investigated the photochemical versus aqueous-phase processing for SOA composition and oxidation degree of OA in summertime Handan, which is a typical industrialized city in the NCP region. The city is located at the intersectional area of Hebei, Shanxi, Henan, and Shandong–four heavily urbanized and industrialized provinces (Fig. S1), and it is therefore an ideal site to investigate the SOA formation pathways in the NCP region. The multiple formation pathways, evolution of SOA composition, and oxidation degree under different meteorological conditions were discussed, which sheds light on the aqueous-phase chemistry and photochemical processing in SOA formation in the NCP region of China.

2. Experimental methods

2.1 Sampling site

Measurements were conducted from 10th August 2019 to 17th September 2019 on the campus of Hebei University of Engineering (36.57 °N, 114.50 °E), located at the southeast edge of urban Handan (Fig. S1). The site is surrounded by a school and residential areas, ~300 m north to South Ring Road and ~400 m northeast to the Handan Highway (S313). The sampling site is on the rooftop of a four-floor building, approximately 12 m above the ground.

2.2 Instrumentation

Real-time non-refractory $PM_{2.5}$ composition was measured by a soot particle long time-of-flight aerosol mass spectrometer (SP-LToF-AMS, Aerodyne Research Inc.) with a time resolution of 1 min. The detailed instrument description and operation of AMS were reported in Onasch et al., (2012). Compared to the conventional AMS, the LToF mass analyzer can provide much better mass resolution of ~8000. During the campaign, the instrument was operated in the "laser off" mode and only the standard tungsten vaporizer was applied. Therefore, only non-refractory $PM_{2.5}$ components (NR-$PM_{2.5}$) were measured, including organics (Org), nitrate (NO3), sulfate (SO4), ammonium (NH4), and chloride (Chl). Ambient air was sampled and dried by a Nafion dryer (MD-700-24S, Perma Pure, Inc.) at a flow rate of 5 L min^{-1}, and then sub-sampled into the SP-LToF-AMS at a flow rate of ~ 0.1 L min^{-1}. An aerodynamic $PM_{2.5}$ lens was used to focus the particle into a beam, which was then impacted on the heated tungsten surface (~ 600 ℃) and flash-vaporized. Electron ionization with 70 eV was used to ionize the vaporized gases. The ionization efficiency (IE) and the relative ionization efficiency (RIE) calibrations (Jimenez et al., 2003) were conducted by using 350 nm ammonium nitrate (NH_4NO_3) and ammonium sulfate ($(NH_4)_2SO_4$) particles.

Gaseous pollutants including SO_2 (9850 SO_2 analyzer, Ecotech), NO_2 (Model 42i NO-NO_2-NO_x analyzer, Thermo Scientific), CO (Model 48i carbon monoxide analyzer, Thermo Scientific), O_3 (Model 49i ozone analyzer, Thermo Scientific), and meteorological parameters including RH and temperature were also measured during the observation period. Furthermore, an aethalometer (Model AE-33, Magee Scientific) was deployed to measure the mass concentration of black carbon (BC) at a time resolution of 1 min.

2.3 Data Analysis

The data analysis software (SQUIRREL, version 1.63I and PIKA, 1.23I) within Igor Pro 6.37 (WaveMetrics) was used to analyze the AMS data. The experimental RIE values of 4 (NH4) and 1.2 (SO4) and the standard RIE values of 1.4 (Org), 1.1 (NO3) and 1.3 (Chl) were used. The composition-dependent collection efficiency (CDCE, Middlebrook et al., 2012) was used to compensate for the incomplete detection caused by particle bounce on the vaporizer. An improved Ambient (I-A) method was adopted for the elemental ratio analysis of high-resolution (HR) OA mass spectra, such as oxygen-to-carbon (O:C), and hydrogen-to-carbon (H:C) ratios (Canagaratna et al., 2015), which reflect the relative composition and oxidation degree for different OA source. In our study, PMF was performed on HR mass spectra of OA for ions with *m/z* values of 12-120, together with the signals from integer *m/z* values between 121 to 300 (i.e., unit mass resolution, UMR) using SoFi (version 6.3) in Igor Pro (Paatero, 1999; Canonaco et al., 2013). The data and error matrices were preprocessed according to Elser et al., (2016) and detailed description of PMF analysis was given elsewhere (Canonaco et al. 2013; Elser et al 2016). Unconstrained PMF solutions with varied factor numbers were analyzed and six factors were resolved, including two primary and four secondary organic factors (Fig. 3). The six-factor solution was preferred because the five-factor solution was not able to separate high signal of *m/z* 44 (which represents high oxidation state) from primary organic aerosol (POA) factors, while the seven-factor solution added additional OOA factors with similar profiles and noisy time series for which no physical interpretation could be found. The two POA factors consisted of a traffic-related factor (hydrocarbon-like OA, HOA) and a cooking-related factor (COA), which had been resolved in previous summer studies in NCP (Elser et al., 2016; Hu et al., 2016b; Sun et al., 2016; Huang et al., 2019). AMS source apportionment studies often report one or two oxygenated organic aerosol (OOA) factors that are distinguished by the extent of oxygenation and linked to volatility or oxidation degree. Owing to higher mass resolution of LTOF-AMS and the inclusion of integer-mass signals for *m/z* from 121 to 300 for high-molecular-weight species such as polycyclic aromatic hydrocarbons (PAHs), we herein resolved four SOA factors. These four SOA factors include aq-SOA attributable to aqueous-phase chemistry, O_x-initiated-SOA attributable to photochemistry, primary-related-SOA attributable to prompt oxidation of POA during emission, and fresh-SOA with a lower f_{44}/f_{43} ratio (fraction of *m/z* 44 and 43 in OA).

2.4 Aerosol liquid water content

The aerosol liquid water content (ALWC) was simulated by ISORROPIA-II model (Fountoukis and Nenes, 2007; Hennigan et al., 2015) using the measurements of ambient inorganic species (NO3, SO4, NH4, and Chl) and meteorological parameters (temperature and RH). The simulation was run in "metastable" mode where all components are assumed to be deliquescent and contain no solid matter. The concentrations and speciation (if dissociated) of those inorganic species in thermodynamic equilibrium was then simulated by the model and then the ALWC was calculated. The ISORROPIA-II model does not consider the contribution to ALWC from organics, since inorganic aerosols dominate the water uptake by ambient particles with a contribution of approximate >80% of the total ALWC (Huang et al., 2020).

3. Results and discussion

3.1 SOA sources

In our study, SOA accounted for 69% (13.5 μg m^{-3}) of the total OA (19.6 μg m^{-3}), representing the dominant fraction in OA in summer Handan. Among the four PMF-resolved SOA sources (Fig. 1), O_x-initiated-SOA dominated (31% to total OA), followed by fresh-SOA (18%), aq-SOA (15%), and primary-related-SOA (5%). Since we focus on SOA formation in this study, detailed descriptions of the HOA (12%) and COA (19%) is provided in section 1.1 in the SI. The mass spectral profiles of the six OA source factors are shown in Fig. 1, while the time series of the SOA factors are shown in Fig. 2. In particular, a remarkable continuous growth of aq-SOA concentration (from ~0.3 μg m^{-3} to 25.2 μg m^{-3}) and ALWC (from 3.1 μg m^{-3} to 486.1 μg m^{-3}) occurred on 24th-28th August (Fig. 2d). Meanwhile, the O:C ratio indicative of OA oxidation state displayed a continuous increase from 0.52 to a maximum of 0.93 during this time (Fig. 2e), consistent with the continuous increase in RH (reaching over 95%). This observation hints that during this period aqueous-phase processing might have played an important role in aq-SOA formation. This role of aqueous-phase processing in SOA formation is not just specific to this particular event, but also important in the whole campaign, which is discussed in detail in section 3.3 later.

SOA factors were resolved depending on the oxidation state, which correspond to aged SOA and fresh SOA respectively (Jimenez et al., 2009). One factor is attributed to aqueous-phase chemistry (aq-SOA) and the other to photochemistry (O_x-initiated-SOA), while fresher factor is produced by fresh-source (fresh-SOA) with a lower f_{44}/f_{43} ratio, and the other considered as oxidized primary sources denoted as primary-related-SOA. Although all of the SOA factors were characterized by higher *m/z* 44 (CO_2^+) and *m/z* 28 (CO^+) signal compared with POA factors, their mass spectrum and temporal trends were noticeably distinguishable,

corresponding to different formation mechanism, which will be discussed in the following section.

As shown in Fig. S3, the aq-SOA was identified as it increased with ALWC but decreased with O_x, which might be produced/influenced by aqueous-phase chemistry and is defined as aq-SOA. This indicates that aq-SOA was either formed via aqueous phase reactions or absorbed/dissolved into aerosol liquid water. It exhibits the highest O:C ratios of all factors (0.7) and a higher f_{CO2+} to the total signal of 21.7%, but a low H:C ratio of 1.24 (Fig. 1). The O_x-initiated-SOA presented an opposite trend with significant increase as function of O_x but decreased as a function of ALWC (Fig. S3) which is defined as O_x-initiated-SOA (influenced by photochemistry). As O_x has been shown to be a conserved tracer to represent photo-oxidation chemistry (Xu et al., 2017), the relationship between O_x and O_x-initiated-SOA can offer insight into the formation mechanism of SOA associated with the progression of atmospheric photochemical aging (Herndon et al., 2008).

The fresh-SOA showed an increase substantially as ALWC increasing, similar to aq-SOA. Whereas it also showed a slight increase trend following O_x when O_x < 100 ppb (Fig. S3). Therefore, both aqueous-phase chemistry and photochemical processing were thought to have positive impacts synchronously on the formation of fresh-SOA. In this study, the fresh-SOA had the lowest atomic O:C ratio of 0.41 and the highest atomic H:C ratio of 1.41 among the four SOA factors, corresponding with the f_{CO2+} of 8.3%, these characteristics are consistent with the global average O:C ratio of LO-OOA of 0.35 ± 0.14, Ng et al., 2010), demonstrating the it is more fresh SOA. Although the primary-related-SOA constituted a small fraction and showed little variation during P1~P3 (3%~5%), this SOA source is also of particular interest because of its distinctive fragments with high *m/z* values in the mass spectrum (Fig. 1d). At *m/z* < 120, the primary-related-SOA had higher intensities for *m/z* 43 (mainly $C_2H_3O^+$) and *m/z* 44 (mainly CO_2^+) than those in POA, indicating a typical nature of less-oxidized SOA. At *m/z* > 120, PAH-derived fragments are clearly evident in the mass spectrum of the primary-related-SOA, as indicated by PAH-like ions (described in SI 1.2) (Dzepina et al., 2007). Previous AMS studies have observed pronounced peaks of PAH ions in POA mass spectra, such as those in coal combustion organic aerosol (CCOA) and biomass burning organic aerosol (BBOA) (Hu et al., 2016b; Zhao et al., 2019), but rarely in SOA. This observation implies that the factor may be related to the POA originated from domestic coal combustion and here it is termed as primary-related-SOA (Xu et al., 2006). Moreover, this SOA factor exhibited relatively better correlations with some gaseous pollutants (Fig. S4), such as CO (R = 0.6) and NO_2 (R = 0.5), and also tracked with HOA (R = 0.4). These observations suggest that the primary-related-SOA might be transformed from locally emitted POA as a non-negligible source to SOA.

To further investigate the SOA formation mechanism, the dataset was segregated into three periods according to different features depends on meteorological parameters (Fig. 2), i.e., the reference period (P1), high-O_x period (P2) and high-RH period (P3). Briefly, the reference period, P1, was characterized by a low average OA concentration (15.4 ± 3.2 μg m^{-3}) and was mainly affected by clean air from southwest of the sampling site and precipitation activities (Table S1). The high-O_x period (P2) was featured by a high O_x concentration (65.1 ± 20.4 ppb), warmer temperatures (26.4 ± 4.0 ℃) but lower RH (57.7 ± 17.5 %). The mass loadings of OA (19.8 ± 4.7 μg m^{-3}) and other pollutants in P2 were higher than those in P1 (Table S1). P3 was assigned as a high-RH period because of the noticeably high RH (83.7 ± 12.5 %) and high ALWC (95.4 ± 114.2 μg m^{-3}). Winds were weak (<1.0 m s^{-1}) throughout this period, indicative of stagnant conditions, which facilitated pollutant accumulation and resulted in the highest average OA concentrations (25.0 ± 6.2 μg m^{-3}).

During the reference period (P1), SOA had the lowest contribution to OA (57%), and the O_x-initiated-SOA and aq-SOA constituted 22% and 21% to total OA, respectively. For the high-O_x period (P2), enhanced SOA formation was found, with the SOA fraction increased to 71% of the total OA. The O_x-initiated-SOA showed the highest mass loading of 7.3 μg m^{-3} and highest contribution of 37% to total OA. These increases suggest that high-O_x condition facilitates the production of SOA by photochemistry, making the O_x-initiated-SOA the major source of SOA during P2. During the high-RH period (P3), SOA fraction continually increased, approaching 79% in total OA, and the SOA was mainly contributed by aq-SOA and fresh-SOA. The mass contribution of aq-SOA increased dramatically from 9% to total OA during P2 to 33% during P3 (Fig. S2), and average mass concentrations from 1.8 μg m^{-3} to 8.3 μg m^{-3}, which suggests rapid SOA production through the aqueous-phase chemistry. Comparatively, the contribution of fresh-SOA was about ~20% in both P2 and P3, but lower in P1 (9%), suggesting that the formation fresh-SOA was affected by both high O_x and high RH. It should also be noted that O:C ratio increased in the succession from P1 (0.73) to P2 (0.74) and further to P3 (0.77), accompanied by continually decrease of H:C ratio from 1.64 to 1.56, and to 1.53 (Fig. 3), suggesting the increase of OA oxidation degree. As a result, the high O_x in P2 and high RH in P3 (as compared to P1) promoted the formation of SOA, specifically O_x-initiated-SOA (in P2) and aq-SOA (in P3), leading to the increase in the degree of oxygenation in total OA.

Overall, our results suggest that SOA could be formed through different pathways, in particular photochemistry, aqueous-phase chemistry, and conversion of POA to SOA contributed to SOA formation.

3.2 Photochemistry

As expected for summertime, photochemistry associated with O_x has significant impacts on the formation and evolution of SOA. Herein, the relationships between OA factors and O_x were investigated to offer insights into the formation mechanisms of SOA associated with the ozone production chemistry (Herndon et al., 2008). During P2, as O_x increased, the mass loadings of O_x-initiated-SOA showed a substantially increasing trend when O_x was > 30 ppb and eventually saturated when O_x was >100 ppb, raising the contribution of O_x-initiated-SOA from 20% to 61% of total OA (Fig. 4). This observation indicates the importance of photochemistry in the formation of O_x-initiated-SOA in summer, in which high O_x concentration as well as temperature corresponding to strong atmospheric oxidative capacity, can accelerate the photochemical formation (Duan et al., 2021). As a comparison, the mass concentrations of other OA factors except O_x-initiated-SOA showed decreasing trends as O_x increased (Fig. 4c). Such differences between SOA factors are likely due to the enhanced secondary production/transformation from POA and fresher SOA factors to the more aged O_x-initiated-SOA. Note that the O:C ratio presented a faster increasing rate as a function of O_x (from 0.6 to 1.0, Fig. 4d) than those in P1 and P3, suggesting that photochemistry might result in higher OA oxidation state during P2.

The typical episode with high-O_x period (P2) was dominated by a series of daytime photochemical evolutions. To evaluate the relative contributions of photochemical and aqueous-phase processing production and the transformation of these SOA factors in different meteorological stages, the average diurnal variations of OA factors, O:C ratios, O_x, temperature, AWLC and primary gas pollutants during different periods are shown for comparison. Fig. 6 shows that O_x increased rapidly from 6:00 to 14:00 in all periods, but was highest in P2. Correspondingly, a lower mean value of ALWC (8.4 $\mu g\ m^{-3}$) was also observed in P2 than in P1 and P3. During P2, O_x-initiated-SOA was produced quickly and played the dominant role during daytime, while its concentration typically decreased during nighttime. The average concentration of O_x-initiated-SOA increased continually from 4.2 $\mu g\ m^{-3}$ at 7:00 local time (LT) to 10.4 $\mu g\ m^{-3}$ at 15:00 LT in 8 h, with the maximum O_x-initiated-SOA mass fraction in OA reaching 65% at 15:00 LT (Fig. S6c). This high average growth rate of 0.8 $\mu g\ m^{-3}\ h^{-1}$ in O_x-initiated-SOA corresponded to the high O_x concentration, high temperature and strong solar radiation in daytime, suggesting enhanced photochemistry reaction. In contrast, the concentrations and the contributions of other SOA factors deceased continuously at the same time (Fig. 6). The opposite trends between O_x-initiated-SOA and other OA factors from 7:00 to 15:00 LT suggest that some part of POA and fresh-SOA may convert to O_x-initiated-SOA by photochemical oxidation. This conclusion is consistent with findings reported by Li et al., (2020) in urban Beijing, where less-oxidized SOA may transform to more-oxidized SOA through photochemical processing as well. The O:C ratio of OA presented a significant increasingly diurnal variation with a noon peak around 14:00 ~ 16:00 LT in P2, which had the

highest value of 0.74 compared with P1 and P3, suggesting the potential transformation from POA factors and fresh SOA factors to O_x-initiated-SOA could also noticeably affect OA characteristics such as oxidation state in summer daytime. It is further indicated by a small afternoon peak of the more oxidized tracer CO_2^+ (*m/z* 44) and the decrease in a less oxidized tracer $C_2H_3O^+$ (*m/z* 43) (Fig. 7b). As a result, the mass spectra, which were initially fresh SOA products evolved to become aged SOA products as the photochemical age increased. Overall, with little water in the particles, the high solar radiation and high O_x concentration during daytime associated with a relatively high degree of oxygenation of OA suggest that gas-phase oxidation and partitioning processes are probably the dominating process in SOA formation during P2.

In addition, these results further support the idea that during the high-O_x period of summer, photochemistry has significant impacts on SOA formation, especially on O_x-initiated-SOA. Note that the role of photochemistry in the formation of O_x-initiated-SOA is not only limited to the gas-phase photochemistry, but also can also occur in the aqueous phase (Kuang et al., 2020). This is the case for P3 in our study, which is discussed further in section 3.3 below.

3.3 Aqueous-phase chemistry

The aqueous-phase chemistry has imposed significant impacts on SOA formation during this field campaign. To further explore the formation mechanism of SOA associated with aqueous-phase chemistry, the relationships between different OA factors and ALWC were investigated. During P3, the mass concentration of aq-SOA increased from 5 μg m^{-3} to 17 μg m^{-3}, yet its fraction showed a particularly pronounced rise from 22.5% to 52% of total OA when ALWC increased from 0.3 to 200 μg m^{-3} (Fig. 5e and f). Note that the strong correlation between aq-SOA and ALWC was not only observed in P3. Rather, the time series of aq-SOA and ALWC were remarkably well correlated throughout the entire campaign (R=0.7, Fig. S4). This general correlation further confirms the important role of aqueous-phase chemistry in the formation of aq-SOA and characterized the aqueous-phase formation of aq-SOA throughout the campaign rather than only in the high-RH event as shown in section 3.1 earlier. We also found that the concentration and fraction of aq-SOA became stable when ALWC was > 200 μg m^{-3}, which is probably attributable to that the aq-SOA formation within droplets was soon outweighed by the scavenging processes when RH was high enough (> 95%). The O:C ratio shows an obvious increase from 0.7 to around 0.85 when ALWC increases to 200 μg m^{-3}, after which it remains relatively stable (0.85) as the ALWC increases further (Fig. 5). These results suggest that aqueous-phase chemistry can affect the oxidation degree of OA by changing SOA composition, especially the enhanced contribution of aq-SOA. However, the growth rate of O:C ratios as ALWC increases in P3 was lower than that in P2 (up to 1 as O_x increases). Also, the correlation between O:C vs. O_x in P2 (R=0.6) was stronger than O:C vs. ALWC (R=0.3) (Fig. S8).

Fig. 6 illustrate the different types of aqueous-phase chemistry in daytime and nighttime. During the nighttime in P3, aqueous-phase oxidation was also enhanced during nighttime (19:00–07:00 LT). As shown in Fig. 6, O:C ratio (0.76) at nighttime in P3 was higher than those in P2, while exhibiting a much smaller peak during daytime. Compared with the low ALWC in P2, the much higher ALWC concentration (peak value of 235.9 μg m^{-3} at 2:00 LT) and higher RH (peak value of 93.7% at 6:00 LT) during nighttime in P3 suggested a dominant contribution by aqueous-phase processing. The aq-SOA shows a quite clear and unique diurnal pattern in P3, with much higher mass concentration during the whole day (especially at nighttime) than those in P1 and P2. After 17:00 LT, aq-SOA started to increase from 4.7 μg m^{-3} to 12.7 μg m^{-3} at 7:00 LT, which showed a rapid nighttime growth rate of 0.6 μg m^{-3} h^{-1}, indicating enhanced SOA formation through aqueous-phase chemistry at night. Whereas O_x-initiated-SOA decreased rapidly from 8.2 μg m^{-3} at 17:00 LT until reaching its lowest concentration of 2.6 μg m^{-3} until the morning, suggesting the gas-to-particle partitioning at night under high ALWC conditions. Furthermore, this transformation could be supported by the increase in CO_2^+ (*m/z* 44) and the decrease in a less oxidized tracer $C_2H_3O^+$ (*m/z* 43) at night (Fig. 7c). Since when the ALWC is sufficiently high, it was likely to accommodate much of the precursor organics and oxidants to low-volatility products through aqueous-phase oxidation. In addition, the dark aqueous-phase SOA formation was likely strong enough to counteract the nighttime scavenging processes under high-RH conditions. Therefore, the dark aqueous-phase chemistry forming aq-SOA shows a dominant role (over 40% to OA) during nighttime in P3.

However, during the daytime, the mass concentration of aq-SOA decreased from 7:00 to 17:00 LT in P3, coinciding an obvious increase trend of O_x-initiated-SOA at the same time with an average growth rate of 0.6 μg m^{-3} h^{-1} (Fig. 6). This phenomenon suggests photochemical processing can also occur in the aqueous phase when RH and ALWC were still high. Photochemical reactions through both aqueous-phase and gas-phase can contribute substantially to the SOA formation in polluted areas of NCP, and during haze days with high RH and ALWC the aqueous-phase photochemical processes played a dominant role in daytime SOA formation (Kuang et al., 2020). The rapid daytime O_x-initiated-SOA formation in our study possibly occurred on the particle surface and in the aerosol liquid water (Ervens et al., 2011) under humid conditions with high ALWC but driven by gas-phase direct photolysis and oxidation by photooxidants under high O_x conditions. Under such high-RH level (RH > 80%), the water-soluble species produced from photochemistry in the gas phase can also partition into the aqueous phase and be further oxidized to form low-volatility products (Carlton et al., 2007; Sullivan et al., 2016). Previous studies have demonstrated that gas-phase oxidants such as OH radicals and H_2O_2 can also partition to the aqueous phase to further oxidize dissolved the oxidized VOCs (OVOCs) into aq-SOA (Ye et al., 2018). Other studies also revealed that photochemical reactions in the aqueous droplets can occur through direct photolysis or through

oxidation by oxidants (Ervens et al., 2011; 2014;Ye et al., 2018). Therefore, in our campaign, dark aqueous-phase chemistry is responsible for rapid aq-SOA formation during nighttime, while the aqueous-phase photochemistry during daytime is likely prevail by rapid daytime O_x-initiated-SOA formation during P3. This comparison demonstrates that the nocturnal aqueous-phase chemistry and daytime aqueous-phase photochemistry are both important pathways in the total SOA growth. The aqueous-phase chemistry related to fresh-SOA is more complicated, requiring both daytime radiative conditions and certain amounts of ALWC in nighttime. For example, Fig. 5e shows that the fresh-SOA has a similar increasing trend with aq-SOA as ALWC increased, however, it also increased slightly as O_x increased (Fig. 4e), hinting that both ALWC and the oxidants are critical for fresh-SOA formation and both the aqueous-phase chemistry and the photochemistry (including that in the aqueous phase) participated to produce fresh-SOA simultaneously. It is worth noting that three peaks were found in the diurnal variation of fresh-SOA in P3. The peaks at around 6:00 and 19:00 LT at night were similar to those of aq-SOA and lower than it, while the peak at around 13:00 LT is consistent with the peak in the diurnal cycle of O_x (Fig. 6). Although there is also a smaller peak around 13:00 LT in P3, the whole pattern of aq-SOA is characterized by decreasing trend at daytime. These results suggest that fresh-SOA could be formed through dark nighttime aqueous-phase reactions, which are partially reversible upon the evaporation of aerosol liquid water, and also formed through photochemical aqueous-phase reactions during daytime. Different from aq-SOA, which is highly correlated and limited with ALWC, two types of aqueous-phase chemistry in daytime and nighttime are dominant pathways to the fresh-SOA growth. Our analysis on formation pathways of these SOA factors suggested the potential interactive roles of gas-phase oxidation, gas-particle partitioning, and aqueous-phase oxidation in the formation of SOA.

3.4 SOA from POA transformation

The photochemistry and aqueous-phase chemistry show distinct effects on POA evolution and SOA formation. The relationships between O_x-initiated-SOA /aq-SOA and other POA-related components (HOA + COA + primary-related-SOA) were plotted in Fig. S9. A strong negative correlation (R=-0.8) between POA-related components and O_x-initiated-SOA was observed (Fig. S9c), consistent with the decrease in mass concentration of POA-related components during P2. This observation suggests that the production of O_x-initiated-SOA was at least partly facilitated by photochemical transformation of other OA components. However, the better diffusion conditions in P2 might also attribute a great extent to the negative correlation, as the formation period of O_x-initiated-SOA usually occurred during the noontime when the boundary layer was much developed, while the POA usually decreased via horizontal and vertical diffusion. In comparison, POA-related components and aq-SOA correlate weakly. When ALWC (<20 μg m^{-3}) and nitrate concentrations were lower (< 3 μg m^{-3}), mostly during

P1 and P2, POA-related components and aq-SOA showed almost no correlation (R=0.1and R=-0.1). However, when ALWC concentration and nitrate concentration were higher than those thresholds above (data points with yellow/red colors mostly during P3), they had a relatively good negative correlation (R=-0.5) (Fig. S9f), indicating the importance of ALWC and nitrate in aqueous-phase chemistry. This is consistent with results in winter Beijing (Wang et al., 2021), where POA factor had strong negative correlations with aq-SOA, suggesting that these POA factors might produce aq-SOA by aqueous-phase oxidation. In addition, under high-ALWC conditions, nitrate had similar formation mechanisms with aq-SOA or high nitrate supports the potential formation/transformation from POA-related components to aq-SOA, which is consistent with the results in section 3.3. The phenomenon of negative correlation between POA-related components and SOA at high O_x/ALWC further emphasizes the importance of conversion from POA to SOA.

As shown in the Van Krevelen (VK) plot (Fig. 8a), O:C and H:C both increase in the succession from primary-related-SOA to O_x-initiated-SOA and eventually to aq-SOA, supporting a successive oxidation sequence from primary-related-SOA to aq-SOA. Generally, H:C shows a decreasing trend as O:C increases for organic compounds during oxidation in other studies (Ng et al., 2011; Gilardoni et al., 2016; Lee et al., 2017: Zhao et al., 2019; Chen et al., 2021), suggesting a general negative correlation between H:C and O:C. This positive relationship of O:C and H:C evolution during oxidative aging in this study is interesting. It might be caused by ring-breaking reactions which could further promote the transformation of aromatic POA to aq-SOA. Previous studies in both laboratory (Huang et al., 2018; Wang et al., 2020) and field (Hu et al., 2016a) demonstrated that the OH-initiated ring-breaking reactions of aromatic species can occur in the aqueous phase and form highly oxidized oxygenated compounds. For example, Hems and Abbatt (2018) suggested that nitrophenol molecules could react rapidly with OH radicals in aqueous solutions with the addition of OH functional groups to the aromatic ring at the initial stage, followed by fragmentation to multifunctional organic species with high H:C and O:C ratios. Wang et al. (2021) found that the ring-breaking oxidation of aromatic FF-POA was the mechanism for aq-SOA formation. Similar to those in primary-related-SOA, PAH-like ions was also found in the mass spectrum of aq-SOA at m/z > 150, albeit less pronounced, consistent with a previous study in Beijing (Wang et al., 2021). This is likely due to the oxidation of PAHs in the conversion of primary-related-SOA and aq-SOA, which is caused by enhanced hydroxylation of the aromatic ring and increased yields of carboxylic acids in OH-initiated reactions (Sun et al., 2010). This kind of ring-breaking oxidation of aromatic POA could thus lead to aq-SOA formation (Huang et al., 2018; Wang et al., 2021). In addition, the locations of aq-SOA and the slope of overall OA are near the line with the slope of -1 in the VK plot, indicating more carboxylic acid formation while the replacement of a hydrogen atom with a carboxylic acid group (−COOH) (Heald et al., 2010;

Ng et al., 2011). This observation supports that oxidation of PAHs was probably involved in the conversion of primary-related-SOA to aq-SOA through aqueous-phase chemistry, leading to functionalization as carbonyls and carboxylic acids.

Specifically, the organic fragments and mass spectrum evolution of OA were analyzed to illuminate the transformation in photochemical processing and aqueous-phase chemistry. Fig. 8b shows the mass fractions of $CH_2O_2^+$, CH_3SO^+, HCO_2^+, and $C_2H_2O_2^+$ ion fragments in OA as a function of ALWC. The aq-SOA was tightly correlated with $CH_2O_2^+$ (R^2 = 0.81) at *m/z* 46 and CH_3SO (R^2 = 0.78) at *m/z* 63 (Fig. S10), Consistently, both of them showed increase trends as ALWC increasing, similar as aq-SOA, which indicating typical fragment characteristics of ions of aqueous-phase processing products (Tan et al., 2009; Sun et al., 2016; Duan et al., 2021). The intensities of HCO_2^+ (*m/z* 45), a common fragment ion of carboxylic acids, is associated with aqueous oxidation of aromatic compounds. $C_2H_2O_2^+$ (*m/z* 58) is a tracer ion for glyoxal, which could be a ring-breaking product from the aqueous-phase oxidation of PAHs. The increasing trends of these ions with ALWC suggest that water-soluble organic species such as carboxylic acids and glyoxal are produced as components of aq-SOA following aromatic oxidation and ring breaking. Moreover, the concentration of PAHs increased with the increase of ALWC (Fig. S11), consistent with the oxidation of PAHs from ring-breaking reactions that can take place in the aqueous phase and being involved in the conversion to aq-SOA.

4. Conclusion

The sources and formation mechanisms of SOA were investigated by online aerosol mass spectrometry and statistical (PMF) analysis from August to September of 2019 in Handan, a mid-sized industrialized city in NCP of China. Four specific SOA factors were resolved, including aq-SOA (15% to total OA), O_x-initiated-SOA (31%), fresh-SOA (18%) and primary-related-SOA (5%). By studying the formation of these SOA factors in different selected periods (P1-P3) against O_x and ALWC, we found multiple pathways leading to their formation, sometimes with mixed pathways for one type of SOA.

Both photochemistry and aqueous-phase chemistry resulted in enhanced OA oxidation state. During high-O_x period, photochemistry had imposed significant impacts on the formation and evolution of SOA in summertime. The O_x-initiated-SOA contributed up to 65% to total OA in the daytime, with a high average growth rate of 0.8 μg m^{-3} h^{-1}, suggesting the efficient daytime formation of SOA from photochemistry. Rapid increases of the concentration and contribution (up to 61%) of O_x-initiated-SOA were found as O_x increased, while all the other OA factors showed decreasing trends with O_x concentration increasing. The difference suggests enhanced secondary transformation from POA/fresh SOA factors to the more aged O_x-initiated-SOA under high-O_x condition. However, during the high-RH period, two types of aqueous-phase

chemistry were both important pathways for the SOA growth. During nighttime and under high-RH conditions, dark aqueous-phase chemistry played significant roles with rapid aq-SOA formation (up to 45% in total OA), while the aqueous-phase photochemistry was more important by rapid O_x-initiated-SOA formation during daytime (up to 39% in total OA). The primary-related-SOA was evidently linked to the POA originated from coal combustion activities, as indicated by the PAH-like ion peaks. Although it constituted a small fraction of 5%, the potential transformation and conversion from primary-related-SOA to aq-SOA could also be an important pathway via hydroxylation of the aromatic ring or ring-breaking oxidation of aromatic POA species through aqueous-phase chemistry. This study highlights the multiple reaction pathways, on top of multiple precursor types, on the SOA formation in industrialized regions, and calls form more in-depth study on the interactive roles of those formation pathways.

Data availability. Raw data used in this study are archived at the Institute of Earth Environment, Chinese Academy of Sciences, and are available on request by contacting the corresponding author.

Supplement. The Supplement related to this article is available online.

Competing interests. The authors declare that they have no conflict of interest.

Author contributions. RJH designed the study. Data analysis and source apportionment were done by YFG and RJH. YFG and RJH wrote the manuscript. YFG and RJH interpreted data and prepared display items. All authors commented on and discussed the manuscript.

Acknowledgement

This work was supported by the National Natural Science Foundation of China (no. 41925015), the Key Research Program of Frontier Sciences from the Chinese Academy of Sciences (no. ZDBS-LY-DQC001), the Strategic Priority Research Program of the Chinese Academy of Sciences (no. XDB40000000), and SKLLQG (no. SKLLQGTD1801).

References

An, Z., Huang, R. J., Zhang, R., Tie, X., Li, G., Cao, J., Zhou, W., Shi, Z., Han, Y., Gu, Z., and Ji, Y.: Severe haze in northern China: A synergy of anthropogenic emissions and atmospheric processes, Proc. Natl. Acad. Sci. U. S. A., 116, 8657–8666, https://doi.org/10.1073/pnas.1900125116, 2019.

Bikkina, S., Kawamura, K., and Sarin, M.: Secondary Organic Aerosol Formation over Coastal Ocean: Inferences from Atmospheric Water-Soluble Low Molecular Weight Organic Compounds, Environ. Sci. Technol., 51, 4347–4357, https://doi.org/10.1021/acs.est.6b05986, 2017.

Canagaratna, M. R., Jimenez, J. L., Kroll, J. H., Chen, Q., Kessler, S. H., Massoli, P., Hildebrandt Ruiz, L., Fortner, E., Williams, L. R., Wilson, K. R., Surratt, J. D., Donahue, N. M., Jayne, J. T., and Worsnop, D. R.: Elemental ratio measurements of organic compounds using aerosol mass spectrometry: Characterization, improved calibration, and implications, Atmos. Chem. Phys., 15, 253–272, https://doi.org/10.5194/acp-15-253-2015, 2015.

Canonaco, F., Crippa, M., Slowik, J. G., Baltensperger, U., and Prévôt, A. S. H.: SoFi, an IGOR-based interface for the efficient use of the generalized multilinear engine (ME-2) for the source apportionment: ME-2 application to aerosol mass spectrometer data, Atmos. Meas. Tech., 6, 3649–3661, https://doi.org/10.5194/amt-6-3649-2013, 2013.

Carlton, A. G., Turpin, B. J., Altieri, K. E., Seitzinger, S., Reff, A., Lim, H. J., and Ervens, B.: Atmospheric oxalic acid and SOA production from glyoxal: Results of aqueous photooxidation experiments, Atmos. Environ., 41, 7588–7602, https://doi.org/10.1016/j.atmosenv.2007.05.035, 2007.

Chen, W., Ye, Y., Hu, W., Zhou, H., Pan, T., Wang, Y., Song, W., Song, Q., Ye, C., Wang, C., Wang, B., Huang, S., Yuan, B., Zhu, M., Lian, X., Zhang, G., Bi, X., Jiang, F., Liu, J., Canonaco, F., Prevot, A. S. H., Shao, M., and Wang, X.: Real-time characterization of aerosol compositions, sources and aging processes in Guangzhou during PRIDE-GBA 2018 campaign, J. Geophys. Res. Atmos., https://doi.org/10.1029/2021jd035114, 2021.

Cohen, A. J., Brauer, M., Burnett, R., Anderson, H. R., Frostad, J., Estep, K., Balakrishnan, K., Brunekreef, B., Dandona, L., Dandona, R., Feigin, V., Freedman, G., Hubbell, B., Jobling, A., Kan, H., Knibbs, L., Liu, Y., Martin, R., Morawska, L., Pope, C. A., Shin, H., Straif, K., Shaddick, G., Thomas, M., van Dingenen, R., van Donkelaar, A., Vos, T., Murray, C. J. L., and Forouzanfar, M. H.: Estimates and 25-year trends of the global burden of disease attributable to ambient air pollution: an analysis of data from the Global Burden of Diseases Study 2015, Lancet, 389, https://doi.org/10.1016/S0140-6736(17)30505-6, 2017.

Donahue, N. M., Robinson, A. L., Stanier, C. O., and Pandis, S. N.: Coupled partitioning, dilution, and chemical aging of semivolatile organics, Environ. Sci. Technol., 40, https://doi.org/10.1021/es052297c, 2006.

539 Duan, J., Huang, R. J., Gu, Y., Lin, C., Zhong, H., Wang, Y., Yuan, W., Ni, H., Yang, L., Chen,
540 Y., Worsnop, D. R., and O'Dowd, C.: The formation and evolution of secondary organic
541 aerosol during summer in Xi'an: Aqueous phase processing in fog-rain days, Sci. Total
542 Environ., 756, 144077, https://doi.org/10.1016/j.scitotenv.2020.144077, 2021.

543 Dzepina, K., Arey, J., Marr, L. C., Worsnop, D. R., Salcedo, D., Zhang, Q., Onasch, T. B.,
544 Molina, L. T., Molina, M. J., and Jimenez, J. L.: Detection of particle-phase polycyclic
545 aromatic hydrocarbons in Mexico City using an aerosol mass spectrometer, Int. J. Mass
546 Spectrom., 263, 152–170, https://doi.org/10.1016/j.ijms.2007.01.010, 2007.

547 Elser, M., Huang, R., Wolf, R., Slowik, J. G., Wang, Q., Canonaco, F., Li, G., Bozzetti, C.,
548 Daellenbach, K. R., Huang, Y., Zhang, R., Li, Z., Cao, J., Baltensperger, U., El-haddad, I.,
549 and Prévôt, A. S. H.: New insights into PM 2 . 5 chemical composition and sources in two
550 major cities in China during extreme haze events using aerosol mass spectrometry, 3207–
551 3225, https://doi.org/10.5194/acp-16-3207-2016, 2016.

552 Ervens, B., Turpin, B. J., and Weber, R. J.: Secondary organic aerosol formation in cloud
553 droplets and aqueous particles (aqSOA): A review of laboratory, field and model studies,
554 Atmos. Chem. Phys., 11, 11069–11102, https://doi.org/10.5194/acp-11-11069-2011, 2011.

555 Ervens, B., Armin, S., B., L. Y., and J., and T. B.: Key parameters controlling OH-initiated
556 formation of secondary organic aerosol in the aqueous phase (aqSOA), J. Geophys. Res.,
557 6578–6595, https://doi.org/10.1002/2013JD021021.Received, 2014.

558 Fountoukis, C. and Nenes, A.: ISORROPIAII: A computationally efficient thermodynamic
559 equilibrium model for K+-Ca2+-Mg2+-NH4+-Na+-SO42--NO3--Cl--H2O aerosols, Atmos.
560 Chem. Phys., 7, 4639–4659, https://doi.org/10.5194/acp-7-4639-2007, 2007.

561 Gilardoni, S., Massoli, P., Paglione, M., Giulianelli, L., Carbone, C., Rinaldi, M., Decesari, S.,
562 Sandrini, S., Costabile, F., and Gobbi, G. P.: Direct observation of aqueous secondary
563 organic aerosol from biomass-burning emissions, Proc. Natl. Acad. Sci. U. S. A., 113,
564 10013–10018, https://doi.org/10.1073/pnas.1602212113, 2016.

565 Gu, Y., Huang, R. J., Li, Y., Duan, J., Chen, Q., Hu, W., Zheng, Y., Lin, C., Ni, H., Dai, W.,
566 Cao, J., Liu, Q., Chen, Y., Chen, C., Ovadnevaite, J., Ceburnis, D., and O'Dowd, C.:
567 Chemical nature and sources of fine particles in urban Beijing: Seasonality and formation
568 mechanisms, Environ. Int., 140, 105732, https://doi.org/10.1016/j.envint.2020.105732,
569 2020.

570 Heald, C. L., Kroll, J. H., Jimenez, J. L., Docherty, K. S., Decarlo, P. F., Aiken, A. C., Chen,
571 Q., Martin, S. T., Farmer, D. K., and Artaxo, P.: A simplified description of the evolution
572 of organic aerosol composition in the atmosphere, Geophys. Res. Lett., 37,
573 https://doi.org/10.1029/2010GL042737, 2010.

574 Hems, R. F. and Abbatt, J. P. D.: Aqueous Phase Photo-oxidation of Brown Carbon
575 Nitrophenols: Reaction Kinetics, Mechanism, and Evolution of Light Absorption, ACS
576 Earth Sp. Chem., 2, 225–234, https://doi.org/10.1021/acsearthspacechem.7b00123, 2018.

Hennigan, C. J., Izumi, J., Sullivan, A. P., Weber, R. J., and Nenes, A.: A critical evaluation of proxy methods used to estimate the acidity of atmospheric particles, Atmos. Chem. Phys., 15, 2775–2790, https://doi.org/10.5194/acp-15-2775-2015, 2015.

Herndon, S. C., Onasch, T. B., Wood, E. C., Kroll, J. H., Canagaratna, M. R., Jayne, J. T., Zavala, M. A., Knighton, W. B., Mazzoleni, C., Dubey, M. K., Ulbrich, I. M., Jimenez, J. L., Seila, R., de Gouw, J. A., de Foy, B., Fast, J., Molina, L. T., Kolb, C. E., and Worsnop, D. R.: Correlation of secondary organic aerosol with odd oxygen in Mexico City, Geophys. Res. Lett., 35, https://doi.org/10.1029/2008GL034058, 2008.

Hu, W., Hu, M., Hu, W. W., Niu, H., Zheng, J., Wu, Y., Chen, W., Chen, C., Li, L., Shao, M., Xie, S., and Zhang, Y.: Characterization of submicron aerosols influenced by biomass burning at a site in the Sichuan Basin, southwestern China, Atmos. Chem. Phys., 16, 13213–13230, https://doi.org/10.5194/acp-16-13213-2016, 2016a.

Hu, W., Hu, M., Hu, W., Jimenez, J. L., Yuan, B., Chen, W., Wang, M., Wu, Y., Chen, C., Wang, Z., Peng, J., Zeng, L., and Shao, M.: Journal of Geophysical Research : Atmospheres, 1955–1977, https://doi.org/10.1002/2015JD024020.Received, 2016b.

Hu, W., Palm, B. B., Day, D. A., Campuzano-Jost, P., Krechmer, J. E., Peng, Z., De Sa Suzane, S., Martin, S. T., Alexander, M. L., Baumann, K., Hacker, L., Kiendler-Scharr, A., Koss, A. R., De Gouw, J. A., Goldstein, A. H., Seco, R., Sjostedt, S. J., Park, J. H., Guenther, A. B., Kim, S., Canonaco, F., Prévôt, A. S. H., Brune, W. H., and Jimenez, J. L.: Volatility and lifetime against OH heterogeneous reaction of ambient isoprene-epoxydiols-derived secondary organic aerosol (IEPOX-SOA), Atmos. Chem. Phys., 16, 11563–11580, https://doi.org/10.5194/acp-16-11563-2016, 2016c.

Hu, W., Hu, M., Hu, W., Zheng, J., Chen, C., Wu, Y., and Guo, S.: Seasonal variations in high time-resolved chemical compositions , sources , and evolution of atmospheric submicron aerosols in the megacity Beijing, 9979–10000, 2017.

Huang, D. D., Zhang, Q., Cheung, H. H. Y., Yu, L., Zhou, S., Anastasio, C., Smith, J. D., and Chan, C. K.: Formation and Evolution of aqSOA from Aqueous-Phase Reactions of Phenolic Carbonyls: Comparison between Ammonium Sulfate and Ammonium Nitrate Solutions, Environ. Sci. Technol., 52, 9215–9224, https://doi.org/10.1021/acs.est.8b03441, 2018.

Huang, R. J., Zhang, Y., Bozzetti, C., Ho, K. F., Cao, J. J., Han, Y., Daellenbach, K. R., Slowik, J. G., Platt, S. M., Canonaco, F., Zotter, P., Wolf, R., Pieber, S. M., Bruns, E. A., Crippa, M., Ciarelli, G., Piazzalunga, A., Schwikowski, M., Abbaszade, G., Schnelle-Kreis, J., Zimmermann, R., An, Z., Szidat, S., Baltensperger, U., El Haddad, I., and Prévôt, A. S. H.: High secondary aerosol contribution to particulate pollution during haze events in China, Nature, 514, 218–222, https://doi.org/10.1038/nature13774, 2014.

Huang, R. J., Wang, Y., Cao, J., Lin, C., Duan, J., Chen, Q., Li, Y., Gu, Y., Yan, J., Xu, W., Fröhlich, R., Canonaco, F., Bozzetti, C., Ovadnevaite, J., Ceburnis, D., Canagaratna, M. R., Jayne, J., Worsnop, D. R., El-Haddad, I., Prevot, A. S. H., and O'Dowd, C. D.: Primary

emissions versus secondary formation of fine particulate matter in the most polluted city (Shijiazhuang) in North China, Atmos. Chem. Phys., 19, 2283–2298, https://doi.org/10.5194/acp-19-2283-2019, 2019.

Huang, R. J., He, Y., Duan, J., Li, Y., Chen, Q., Zheng, Y., Chen, Y., Hu, W., Lin, C., Ni, H., Dai, W., Cao, J., Wu, Y., Zhang, R., Xu, W., Ovadnevaite, J., Ceburnis, D., Hoffmann, T., and D. ODowd, C.: Contrasting sources and processes of particulate species in haze days with low and high relative humidity in wintertime Beijing, Atmos. Chem. Phys., 20, 9101–9114, https://doi.org/10.5194/acp-20-9101-2020, 2020.

Jimenez, J. L., Jayne, J. T., Shi, Q., Kolb, C. E., Worsnop, D. R., Yourshaw, I., Seinfeld, J. H., Flagan, R. C., Zhang, X., Smith, K. A., Morris, J. W., and Davidovits, P.: Ambient aerosol sampling using the Aerodyne aerosol mass spectrometer, J. Geophys. Res. Atmos., 108, 1–13, https://doi.org/10.1029/2001jd001213, 2003.

Jimenez, J. L., Canagaratna, M. R., Donahue, N. M., Prevot, A. S. H., Zhang, Q., Kroll, J. H., DeCarlo, P. F., Allan, J. D., Coe, H., Ng, N. L., Aiken, A. C., Docherty, K. S., Ulbrich, I. M., Grieshop, A. P., Robinson, A. L., Duplissy, J., Smith, J. D., Wilson, K. R., Lanz, V. A., Hueglin, C., Sun, Y. L., Tian, J., Laaksonen, A., Raatikainen, T., Rautiainen, J., Vaattovaara, P., Ehn, M., Kulmala, M., Tomlinson, J. M., Collins, D. R., Cubison, M. J., Dunlea, E. J., Huffman, J. A., Onasch, T. B., Alfarra, M. R., Williams, P. I., Bower, K., Kondo, Y., Schneider, J., Drewnick, F., Borrmann, S., Weimer, S., Demerjian, K., Salcedo, D., Cottrell, L., Griffin, R., Takami, A., Miyoshi, T., Hatakeyama, S., Shimono, A., Sun, J. Y., Zhang, Y. M., Dzepina, K., Kimmel, J. R., Sueper, D., Jayne, J. T., Herndon, S. C., Trimborn, A. M., Williams, L. R., Wood, E. C., Middlebrook, A. M., Kolb, C. E., Baltensperger, U., and Worsnop, D. R.: Evolution of organic aerosols in the atmosphere, Science (80-.)., 326, 1525–1529, https://doi.org/10.1126/science.1180353, 2009.

Kuang, Y., He, Y., Xu, W., Yuan, B., Zhang, G., Ma, Z., Wu, C., Wang, C., Wang, S., Zhang, S., Tao, J., Ma, N., Su, H., Cheng, Y., Shao, M., and Sun, Y.: Photochemical Aqueous-Phase Reactions Induce Rapid Daytime Formation of Oxygenated Organic Aerosol on the North China Plain, Environ. Sci. Technol., 54, 3849–3860, https://doi.org/10.1021/acs.est.9b06836, 2020.

Lee, A. K. Y., Chen, C. L., Liu, J., Price, D. J., Betha, R., Russell, L. M., Zhang, X., and Cappa, C. D.: Formation of secondary organic aerosol coating on black carbon particles near vehicular emissions, Atmos. Chem. Phys., 17, 15055–15067, https://doi.org/10.5194/acp-17-15055-2017, 2017.

Li, H., Zhang, Q., Zhang, Q., Chen, C., Wang, L., Wei, Z., Zhou, S., Parworth, C., Zheng, B., Canonaco, F., Prévôt, A. S. H., Chen, P., Zhang, H., Wallington, T. J., and He, K.: Wintertime aerosol chemistry and haze evolution in an extremely polluted city of the North China Plain: Significant contribution from coal and biomass combustion, Atmos. Chem. Phys., 17, 4751–4768, https://doi.org/10.5194/acp-17-4751-2017, 2017.

Li, J., Liu, Z., Gao, W., Tang, G., Hu, B., Ma, Z., and Wang, Y.: Insight into the formation and evolution of secondary organic aerosol in the megacity of Beijing, China, Atmos. Environ., 220, https://doi.org/10.1016/j.atmosenv.2019.117070, 2020.

Middlebrook, A. M., Bahreini, R., Jimenez, J. L., and Canagaratna, M. R.: Evaluation of composition-dependent collection efficiencies for the Aerodyne aerosol mass spectrometer using field data, Aerosol Sci. Technol., 46, 258–271, https://doi.org/10.1080/02786826.2011.620041, 2012.

Ng, N. L., Canagaratna, M. R., Zhang, Q., Jimenez, J. L., Tian, J., Ulbrich, I. M., Kroll, J. H., Docherty, K. S., Chhabra, P. S., Bahreini, R., Murphy, S. M., Seinfeld, J. H., Hildebrandt, L., Donahue, N. M., Decarlo, P. F., Lanz, V. A., Prévôt, A. S. H., Dinar, E., Rudich, Y., and Worsnop, D. R.: Organic aerosol components observed in Northern Hemispheric datasets from Aerosol Mass Spectrometry, Atmos. Chem. Phys., 10, 4625–4641, https://doi.org/10.5194/acp-10-4625-2010, 2010.

Ng, N. L., Canagaratna, M. R., Jimenez, J. L., Chhabra, P. S., Seinfeld, J. H., and Worsnop, D. R.: Changes in organic aerosol composition with aging inferred from aerosol mass spectra, Atmos. Chem. Phys., 11, 6465–6474, https://doi.org/10.5194/acp-11-6465-2011, 2011.

Onasch, T. B., Trimborn, A., Fortner, E. C., Jayne, J. T., Kok, G. L., Williams, L. R., Davidovits, P., and Worsnop, D. R.: Soot particle aerosol mass spectrometer: Development, validation, and initial application, Aerosol Sci. Technol., 46, 804–817, https://doi.org/10.1080/02786826.2012.663948, 2012.

Paatero, P.: The Multilinear Engine—A Table-Driven, Least Squares Program for Solving Multilinear Problems, Including the n-Way Parallel Factor Analysis Model, J. Comput. Graph. Stat., 8, 854–888, https://doi.org/10.1080/10618600.1999.10474853, 1999.

Sullivan, A. P., Hodas, N., Turpin, B. J., Skog, K., Keutsch, F. N., Gilardoni, S., Paglione, M., Rinaldi, M., Decesari, S., Cristina Facchini, M., Poulain, L., Herrmann, H., Wiedensohler, A., Nemitz, E., Twigg, M., and Collett, J. L.: Evidence for ambient dark aqueous SOA formation in the Po Valley, Italy, Atmos. Chem. Phys., 16, 8095–8108, https://doi.org/10.5194/acp-16-8095-2016, 2016.

Sun, Y., Chen, C., Zhang, Y., Xu, W., Zhou, L., Cheng, X., Zheng, H., Ji, D., Li, J., Tang, X., Fu, P., and Wang, Z.: Rapid formation and evolution of an extreme haze episode in Northern China during winter 2015, 1–9, https://doi.org/10.1038/srep27151, 2016.

Sun, Y., Xu, W., Zhang, Q., Jiang, Q., Canonaco, F., Prévôt, A. S. H., Fu, P., Li, J., Jayne, J., Worsnop, D. R., and Wang, Z.: Source apportionment of organic aerosol from 2-year highly time-resolved measurements by an aerosol chemical speciation monitor in Beijing, China, Atmos. Chem. Phys., 18, 8469–8489, https://doi.org/10.5194/acp-18-8469-2018, 2018a.

Sun, Y., Xu, W., Zhang, Q., Jiang, Q., Canonaco, F., and Prévôt, A. S. H.: Source apportionment of organic aerosol from two-year highly time- resolved measurements by an aerosol chemical speciation monitor in Beijing , China, 2018b.

692 Sun, Y. L., Zhang, Q., Anastasio, C., and Sun, J.: Insights into secondary organic aerosol
693 formed via aqueous-phase reactions of phenolic compounds based on high resolution mass
694 spectrometry, Atmos. Chem. Phys., 10, 4809–4822, https://doi.org/10.5194/acp-10-4809-
695 2010, 2010.

696 Wang, J., Ye, J., Zhang, Q., Zhao, J., Wu, Y., Li, J., Liu, D., Li, W., Zhang, Y., Wu, C., Xie,
697 C., Qin, Y., Lei, Y., Huang, X., Guo, J., Liu, P., Fu, P., Li, Y., Lee, H. C., Choi, H., Zhang,
698 J., Liao, H., Chen, M., Sun, Y., Ge, X., Martin, S. T., and Jacob, D. J.: Aqueous production
699 of secondary organic aerosol from fossil-fuel emissions in winter Beijing haze, Proc. Natl.
700 Acad. Sci. U. S. A., 118, 1–6, https://doi.org/10.1073/pnas.2022179118, 2021.

701 Wang, S., Newland, M. J., Deng, W., Rickard, A. R., Hamilton, J. F., Muñoz, A., Ródenas, M.,
702 Vázquez, M. M., Wang, L., and Wang, X.: Aromatic Photo-oxidation, A New Source of
703 Atmospheric Acidity, Environ. Sci. Technol., 54, 7798–7806,
704 https://doi.org/10.1021/acs.est.0c00526, 2020.

705 Xu, S., Liu, W., and Tao, and S.: Emission of Polycyclic Aromatic Hydrocarbons in China,
706 Biophys. Process. Anthropog. Org. Compd. Environ. Syst., 40, 267–281,
707 https://doi.org/10.1002/9780470944479.ch11, 2006.

708 Xu, W., Han, T., Du, W., Wang, Q., Chen, C., Zhao, J., Li, J., Fu, P., Wang, Z., Worsnop, D.
709 R., and Sun, Y.: Effects of Aqueous-phase and Photochemical Processing on Secondary
710 Organic Aerosol Formation and Evolution in Beijing , China,
711 https://doi.org/10.1021/acs.est.6b04498, 2017.

712 Xu, W., Sun, Y., Wang, Q., Zhao, J., Wang, J., Ge, X., Xie, C., Zhou, W., Du, W., Li, J., Fu,
713 P., Wang, Z., Worsnop, D. R., and Coe, H.: Changes in Aerosol Chemistry From 2014 to
714 2016 in Winter in Beijing: Insights From High-Resolution Aerosol Mass Spectrometry, J.
715 Geophys. Res. Atmos., 124, 1132–1147, https://doi.org/10.1029/2018JD029245, 2019.

716 Ye, C., Liu, P., Ma, Z., Xue, C., Zhang, C., Zhang, Y., Liu, J., Liu, C., Sun, X., and Mu, Y.:
717 High H2O2 Concentrations Observed during Haze Periods during the Winter in Beijing:
718 Importance of H2O2 Oxidation in Sulfate Formation, Environ. Sci. Technol. Lett., 5, 757–
719 763, https://doi.org/10.1021/acs.estlett.8b00579, 2018.

720 Zhang, Q., Jimenez, J. L., Canagaratna, M. R., Ulbrich, I. M., Ng, N. L., Worsnop, D. R., and
721 Sun, Y.: Understanding atmospheric organic aerosols via factor analysis of aerosol mass
722 spectrometry: A review, https://doi.org/10.1007/s00216-011-5355-y, 2011.

723 Zhao, J., Qiu, Y., Zhou, W., Xu, W., Wang, J., Zhang, Y., Li, L., Xie, C., Wang, Q., Du, W.,
724 Worsnop, D. R., Canagaratna, M. R., Zhou, L., Ge, X., Fu, P., Li, J., Wang, Z., Donahue, N.
725 M., and Sun, Y.: Organic Aerosol Processing During Winter Severe Haze Episodes in
726 Beijing, J. Geophys. Res. Atmos., 124, 10248–10263,
727 https://doi.org/10.1029/2019JD030832, 2019.

728

Figures

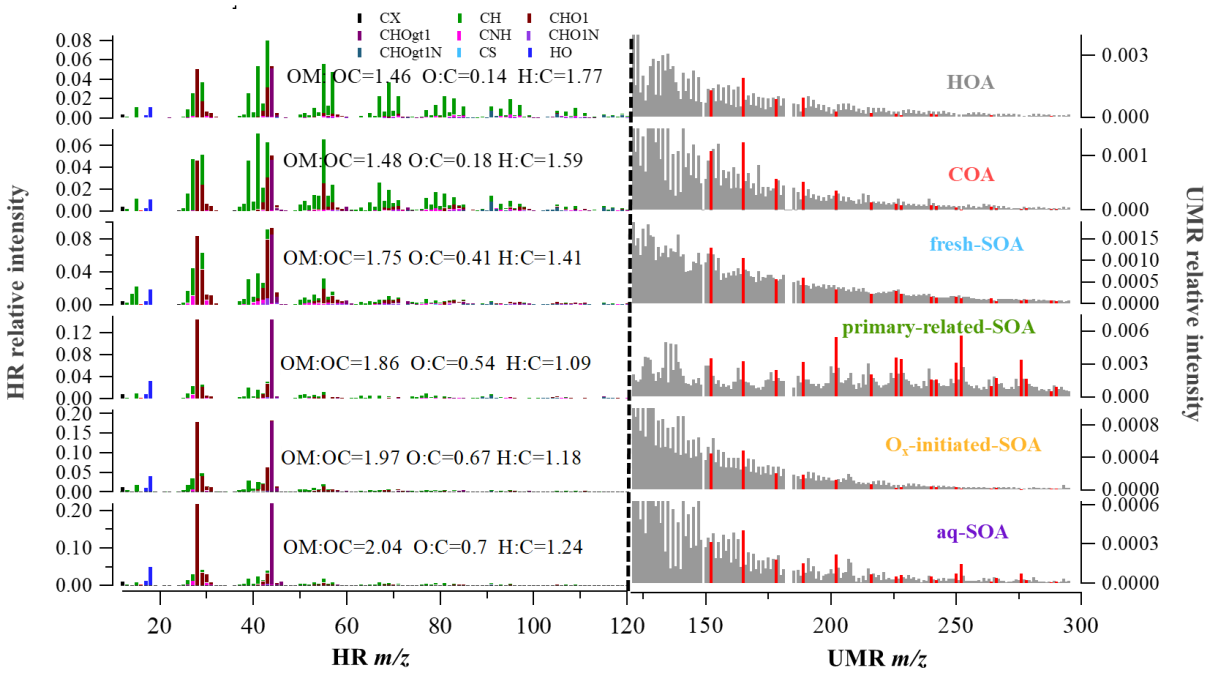

Fig. 1 HR and UMR mass spectra of OA factors: (a) HOA; (b) COA; (c) fresh-SOA; (d) primary-related-SOA; (e) O_x-initiated-SOA; (f) aq-SOA. Mass spectra signals less than 120 amu are colored by nine ion categories, signals equal to or greater than 120 amu are in unit mass resolution, and polycyclic aromatic hydrocarbons (PAHs) signals are in red on the right panels.

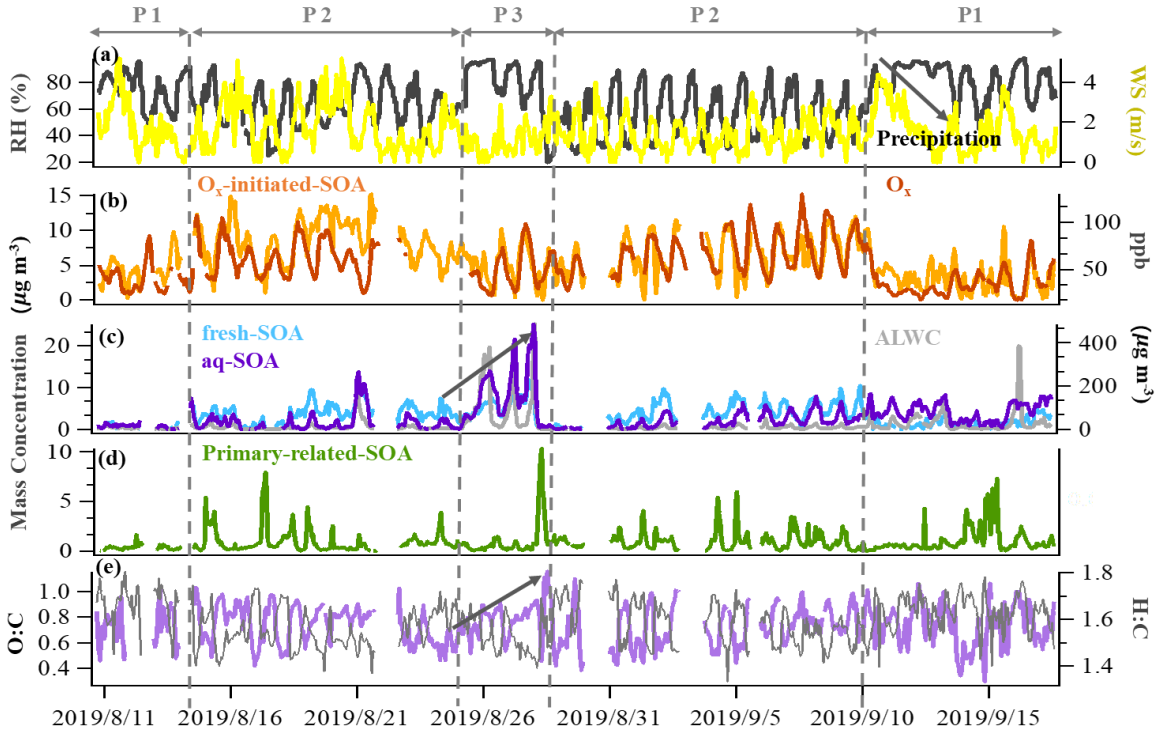

741

742 **Fig. 2** Time series of (a) relative humidity (RH) and wind speed (WS), (b) O_x and O_x-initiated-
743 SOA, (c) fresh-SOA, aq-SOA and ALWC, (d) primary-related-SOA, (e) the O:C ratio and H:C
744 ratio. The time series were categorized to be three typical periods based on total SOA mass
745 concentrations and meteorology conditions: reference period (P1), high O_x period (P2) and high
746 RH period (P3).

747

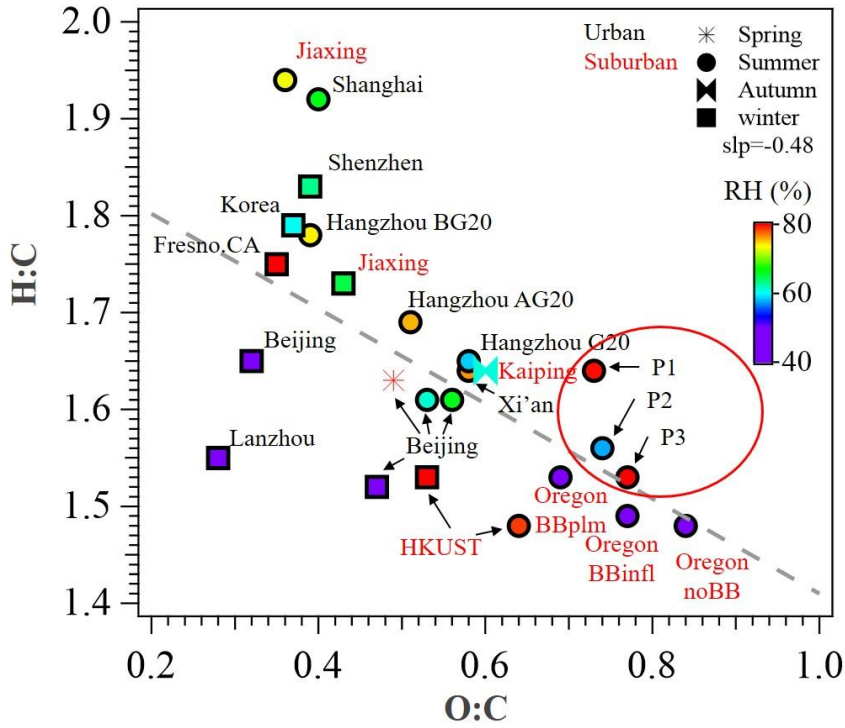

748

749 **Fig.3** Van Krevelen plot for OA of urban and suburban sites in China and other nations. Data
750 points are colored by RH (%). P1, P2 and P3 in red circles represents the different periods in
751 this study. All the data and related references can be found in Table S3.

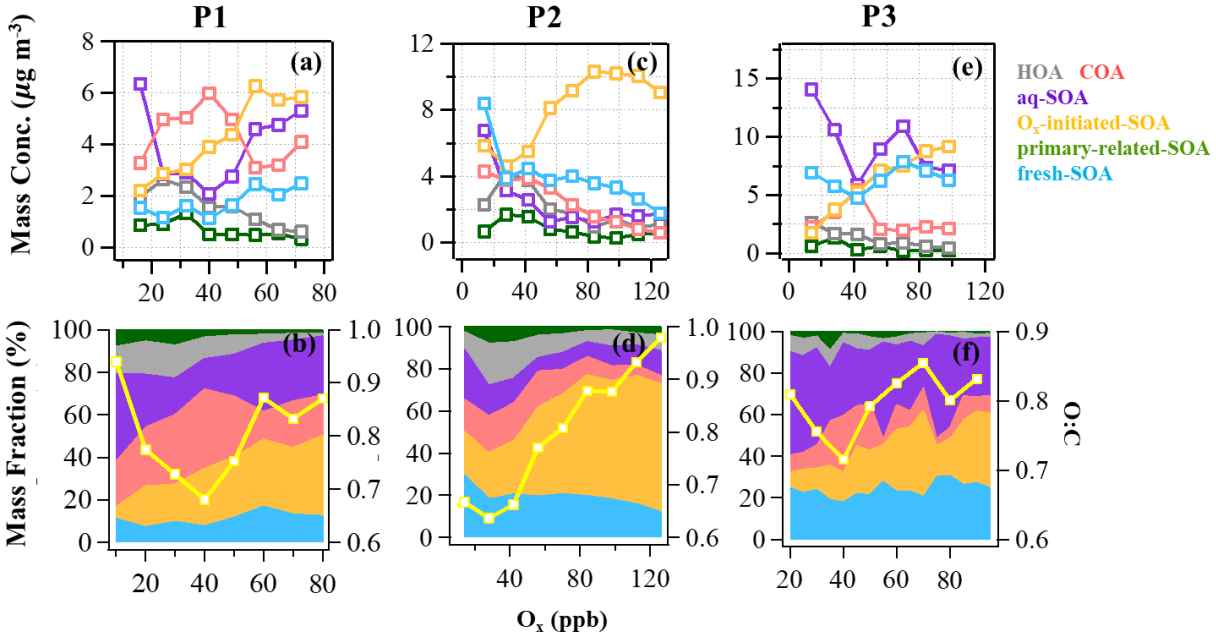

752

753 **Fig. 4** The mass concentration and contribution of OA factors as functions of O_x in reference
754 period (P1: a & b), high O_x period (P2: c & d) and high RH period (P3: e & f) during this

campaign. The yellow curves represent the O:C ration vs. O_x. The data were binned according to O_x concentration (10 ppb increment in P1, 20 ppb increment in P2 and P3).

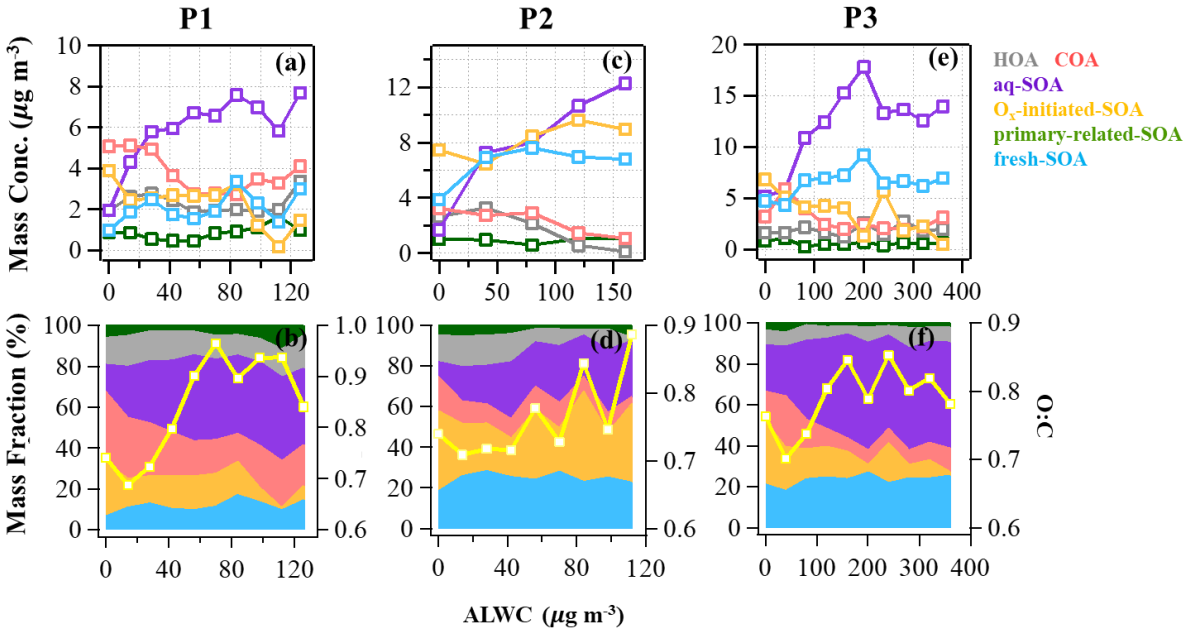

Fig. 5 The mass concentration and contribution of OA factors as functions of ALWC in reference period (P1: a & b), high O_x period (P2: c & d) and high RH period (P3: e & f) during this campaign. The yellow curves represent the O:C ration v.s. ALWC. The data were binned according to the ALWC concentration (20 μgm^{-3} increment in P1 and P2, 50 μgm^{-3} increment in P3).

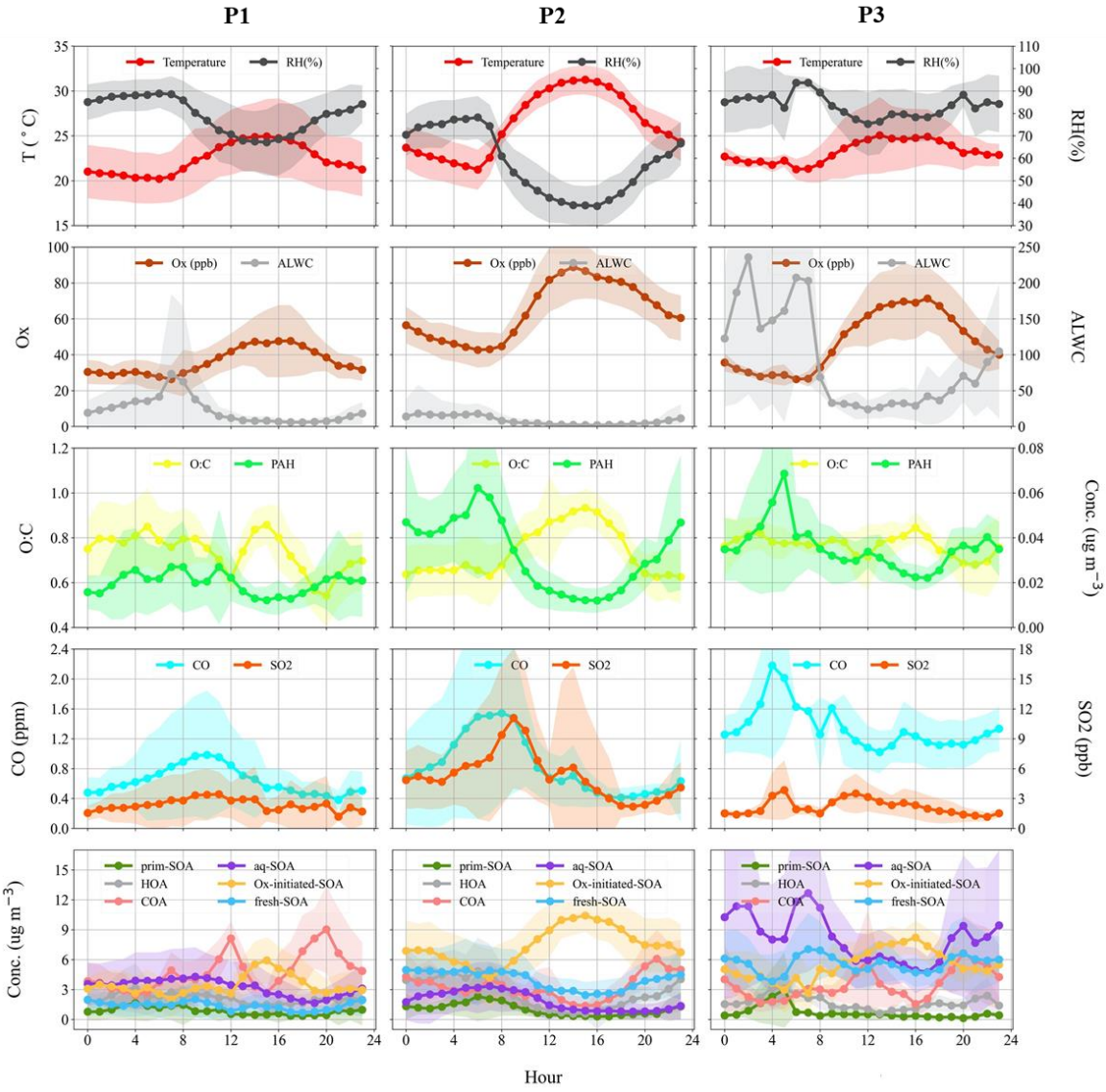

Fig. 6 Diurnal patterns of meteorological parameters (T, RH), gaseous species (O_x, CO, SO_2), ALWC (liquid water content), O:C (oxygen-to-carbon elemental ratio), polycyclic aromatic hydrocarbons (PAHs) fragments and OA factors in reference period (P1), high O_x period (P2) and high RH period (P3) in this campaign.

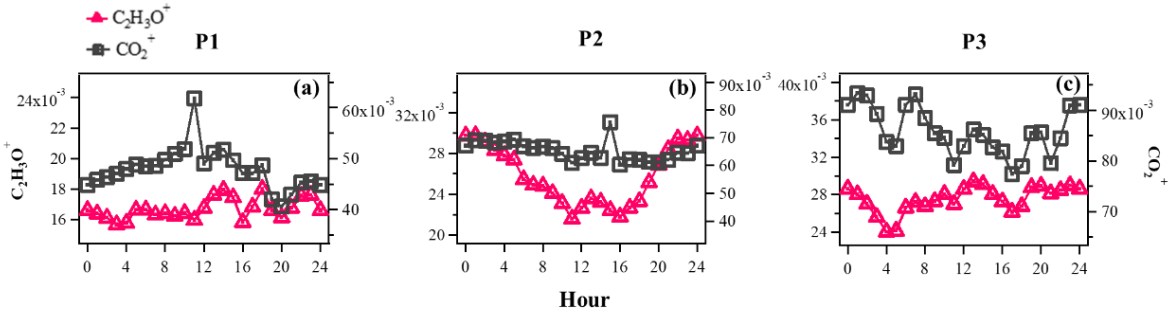

Fig. 7 Evolution of high-resolution organic mass spectra on changes in relative intensities (mass fraction) of oxygen-containing ions: $C_2H_3O^+$ (*m/z* 43) and CO_2^+ (*m/z* 44) in reference period (P1:a), high O_x period (P2: b) and high RH period (P3: c) in this campaign.

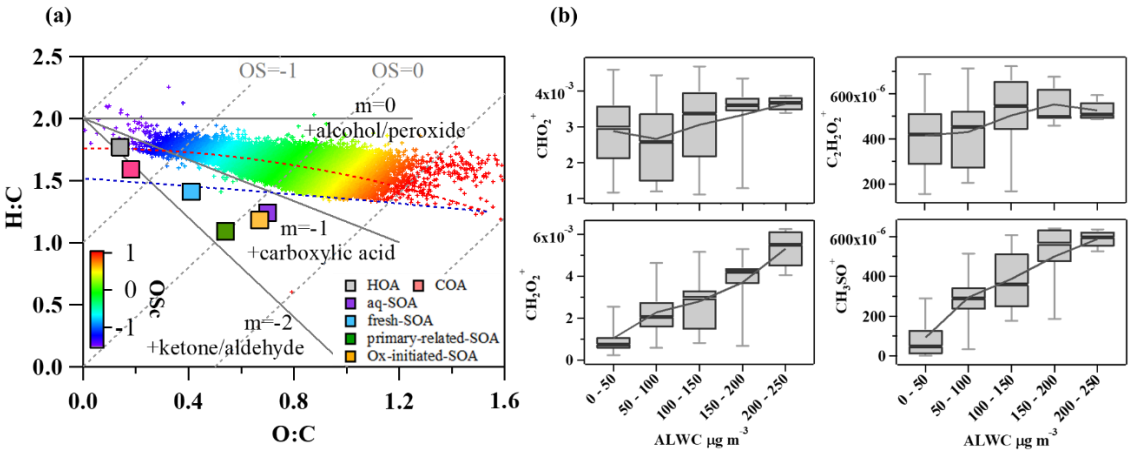

Fig. 8 (a) Van Krevelen diagram for the O:C and H:C ratios of different OA factors (marked with squares) and bulk of OA during summer (marked with plus signs and colored by Osccarbon oxidation state (OSc)); (b) Mass fractions of ion fragments indicative of aqueous-phase processing and oxygenated functional groups (alcohols, carboxylic acids) as a function of ALWC.